COMPARISON OF QUASI-SPECULAR RADAR SCATTER FROM THE MOON WITH SURFACE PARAMETERS OBTAINED FROM IMAGES

(NASA-CR-155713) COMPARISON OF QUASI-SPECULAR RADAR SCATTER FROM THE MOON WITH SURFACE PARAMETERS OBTAINED FROM IMAGES (Stanford Univ.) 53 p HC A04/MF A01 CSCL 03B G3/91

N78-17972

Unclas 04451

G. Leonard Tyler
Center for Radar Astronomy
Stanford University
Stanford, CA 94305

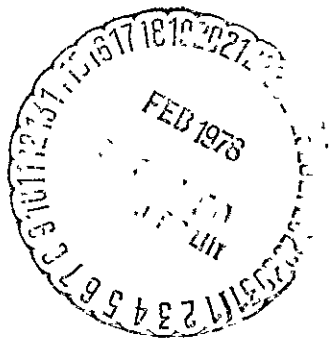

January 9, 1978

Running caption: "Comparison of radar and images"

Address editorial correspondance to:

G. Leonard Tyler
Center for Radar Astronomy
Stanford University, CA 94305

Double underline indicates first reference to a table or figure.

48 pages
5 figures

ABSTRACT

Quasi-specular radar scatter from geologic surfaces displays a variable wavelength, λ, dependence in apparent surface roughness, σ_x, ranging between $\sigma_x \sim \lambda^0$ and $\sigma_x \sim \lambda^{-1/3}$, for $.01 \lesssim \lambda \lesssim 1$ m. The strongest changes in σ_x with wavelength are observed in lunar mare, while scatter from lunar highlands and most of Mars' equatorial region is wavelength independent. Commonly used, gently-undulating surface models for electromagnetic scatter predict no wavelength dependence. Wavelength dependence will occur whenever a significant fraction of the surface has local radii of curvature comparable to the observing wavelength. This condition can be determined by comparison of the value of the integrated surface curvature spectrum with the radar wavenumber, multiplied by a constant that depends on the geometry.

Variations in curvature statistics calculated from photogrammetric reduction of lunar images are consistent with the observed variations in quasi-specular scatter at the same locations. Variations in the strength of the wavelength dependence are correlated with the sizes of lunar craters that lie near the upper size limit for the local steady state distribution. This correlation is also consistent with variations in the curvature spectrum calculated from crater size-frequency distributions.

Introduction

Earth-based radar observations of the moon and terrestrial planets are dominated by a small area of intense scattering in the center of the planetary disk (Evans, 1969). Similar observations that use space probes to achieve oblique-scattering, or bistatic, geometries give equivalent results in which the strong scattering area is always approximately centered on the point where the angles of incidence and reflection are equal with respect to the mean surface (Tyler and Howard, 1973). Earth-based observations represent the special case of normal incidence and reflection. The polarized scatter from the dominant bright area is termed quasi-specular.

The scatter from portions of the surface that do not approximate the specular conditions is observed to be insensitive to the detailed geometry, and is termed diffuse. Diffuse scatter generally obtains in radar mapping from the earth where backscatter at moderate to high angles of incidence is employed. Quasi-specular scatter is dominant in studies of scattering laws for the moon and planets, in oblique scatter experiments, and in radar studies of Mars, where fundamental sampling considerations limit earth-based analyses to a small area surrounding the sub-radar point. Only quasi-specular scatter is considered in this paper.

Quasi-specular scatter can be modeled by random surface models which have considerable roughness on scales that are much larger than the radar wavelength. That is, both the horizontal and vertical roughness scales are many wavelengths in extent. Sub-surface reflections, shadowing, and

edge effects can be shown to be unimportant for many practical cases, and are neglected. Typically, these surfaces are characterized as gently undulating. The principal contribution to the scattering from such surfaces arises from those points on the surface where the local slopes are properly oriented to produce a specular ray path -- angle of incidence equals angle of reflection -- between the radar transmitter and receiver, whether these are co-located or separate. The assumption that the surface roughness scales are large with respect to the radar wavelength leads to the analytical result that scatter from gently undulating surfaces should be wavelength independent.

Quasi-specular radiowave scattering from lunar and planetary surfaces is variable in its behavior with wavelength. Quasi-specular scatter from lunar plains units consistently reveals a strong wavelength dependence in apparent surface roughness over the range of centimeter to meter wavelengths, while most other lunar units show little or no variation in quasi-specular scatter with wavelengths in this range (Tyler and Howard, 1973). Measurements of lunar samples show the electrical properties of the rocks to be nearly constant over this wavelength range. With a few exceptions, radiowave scatter from the equatorial region of Mars also appears to be independent of wavelength within this range (Downs, et al., 1975; Downs et al., 1978; Simpson et al., 1977). Except for the observed variation with wavelength, the quasi-specular scatter from lunar plains is indistinguishable from other lunar units, or Mars, or from expectations based on theory. These other surfaces do exhibit somewhat different radar slope frequency distributions, however. The variations in radar roughness with wavelength correlate well with similar variations in photogrammetric roughness with sampling scale.

Wavelength variability has been discussed generally in terms of a filtering property of the scattering process wherein the quasi-specular scatter is unaffected by surface structure which is small with respect to a wavelength (Hagfors, 1966). We have attempted in a previous paper (Tyler, 1976, afterwards called Paper I) to give quantitative definition to this process by estimating the conditions under which a real surface is statistically equivalent to the type of surface assumed in the models of quasi-specular theory. Real surfaces that are well approximated in this sense are expected to display little or no wavelength dependence in radar properties, while those that violate the modeling assumptions are expected to display some variation in radar characteristics with wavelength. Very little other work in this area has been carried out.

In the remainder of this paper we discuss a comparison between the observed wavelength dependence in lunar radar scatter data and statistical measures of the surface derived from orbital images. Two types of comparison are possible. First, at a limited number of locations we are able, through the use of photogrammetrically determined heights, to calculate the distributions of height variance with inverse lateral surface scales, or frequencies. The surface roughness parameters that are important in determining wavelength dependence are calculated from these distributions. Results of these calculations are compared with oblique-scatter bistatic-radar results from the same location on the moon, or from within a contiguous, independently mapped geologic unit. This comparison suffers primarily from inadequate surface resolution in the orbital images which leads to an extrapolation of the height-variance spectra to small scales. The second method is based

upon a statistical model of lunar surface erosion that is used to determine relative surface ages. The frequency-size distributions of lunar craters in plains units are well behaved, and characterized by a particular crater diameter, C_s, that separates the members of the "old", and "new" or "steady state," crater populations. This crater diameter is readily determined from images. The observed crater populations can be related to the height variance spectrum theoretically through the model. Again, the height-variance spectrum can be related to the expected behavior with wavelength. Bistatic-radar data are used for the comparison. This method suffers from area sampling problems associated with the determination of C_s, and the requirement for other assumptions that have not been tested. However, the model on which it is based has been validated to lateral scales of 10 cm or less by direct observations of the surface at Surveyor and Apollo landing sites, and thus is applicable directly to the surface scales of concern here.

More thorough discussions of quasi-specular scatter and its relationship to planetary radar data can be found in Paper I and elsewhere (e.g., Beckmann, 1963; Hagfors, 1966; Barrick, 1968, 1970; Evans, 1969). Radar procedures and results used here have been described by Tyler and Howard (1973), and by Tyler et al., 1973). Detailed comparisons of oblique-scatter radar data with other remote sensing data are also of interest in understanding the importance of various geologic surface expressions on radar scatter, and are given elsewhere (Moore et al. 1975, 1976).

Requirements for Radar Model

Consider a two-dimensional surface, $\zeta(x,y)$, generated by an isotropic gaussian random process with mean zero, $\langle \zeta \rangle = 0$, and mean square height, $\langle \zeta^2 \rangle = h_o^2$. Let $R_{\zeta\zeta}(\tau) = R(\tau)$ represent the surface height correlation function evaluated at separation $\tau = [(x_1-x_2)^2 + (y_1-y_2)^2]^{1/2}$. The quantities

$$R_{\zeta_x\zeta_x}(0) = \sigma_x^2 = \sigma_y^2$$

$$R_{\zeta_{xx}\zeta_{xx}}(0) = \sigma_{xx}^2 = \sigma_{yy}^2$$

are the variances $\frac{\partial \zeta}{\partial x}$ and $\frac{\partial^2 \zeta}{\partial x^2}$, respectively. These quantities can be expressed as weighted integrals of the surface height-variance spectrum,

$$\sigma_x^2 = \sigma_x^2 = 4\pi^3 \int_0^\infty q^3 S(q)dq$$

$$= \sigma_t^2/2 = \langle \tan^2\gamma \rangle /2 \qquad (1)$$

$$\sigma_{xx}^2 = \sigma_{yy}^2 = 12\pi^5 \int_0^\infty q^5 S(q)dq$$

where σ_t^2 is the variance of the total slope or surface tilt, and the height-variance spectrum,

$$S(q) = 2\pi \int_0^\infty R(\tau)\, J_o(2\pi\tau q)\tau d\tau$$

and autocorrelation function (2)

$$R(\tau) = 2\pi \int_0^\infty S(q)\, J_o(2\pi\tau q) q d\tau$$

form a Hankel transform pair. We refer to $q^3S(q)$ and $q^5S(q)$ as slope and curvature spectra, respectively.

Electromagnetic models for gently undulating surfaces always assume that the radius of curvature of the surface is everywhere much larger than the wavelength of interest. Paper I gives the probability distribution of surface curvature at the local specular points as,

$$P(|r_{12}^2| \leq \hat{r}_{12}^2) \simeq$$

$$2.8\left[\operatorname{erfc}\left(\frac{1.5}{\mu}\right)^{1/2} + .71\ \operatorname{erfc}\left(\frac{3.0}{\mu}\right)^{1/2} + .87\ \exp\left(\frac{-3.0}{\mu}\right)\right]; \qquad (3)$$

$$\mu = 2\,\hat{r}_{12}^2\,\sigma_{xx}^2\cos^4\gamma \gtrsim 4$$

where r_{12}^2 is the product of the principal radii of curvature, and γ is the tilt of the local surface at the specular point. This function is plotted in Figure 1. The probability that $|r_{12}^2|$ exceeds some particular value $\hat{r}_{12}^2$ is a very rapidly decreasing function of μ, for values of μ less than about 1. The model will closely approximate the real surface, and vice versa, if $P(|r_{12}^2| \leq \hat{r}_{12}^2)$ is very small for an appropriate choice of threshold curvature, $\hat{r}_{12}^2$.

If the height variance spectrum is known to scales significantly less than a wavelength the value of $P(\cdot)$ can be estimated. The quantity σ_{xx}^2 is easily obtained from (1), while $\cos\gamma \simeq 1$ for quasi-specular scatter. In our previous discussion we suggested that the Rayleigh criterion $\hat{r}_{12}^2 \gtrsim \kappa^{-2} = \left(\frac{\lambda}{2\pi}\right)^2$, where λ is the radar wavelength, provides a firm lower bound on the radius of curvature. With these substitutions the parameter μ becomes

$$\mu \simeq \frac{\lambda^2}{2\pi^2}\,\sigma_{xx}^2, \tag{4}$$

which depends only on the wavelength and the curvature spectrum.

The infinite upper bound in the computation of σ_{xx}^2 is not strictly required, because it is known that roughness on very small scales with respect to a wavelength does not affect the specular scatter significantly (Barrick, 1970). Thus, σ_{xx}^2 can be replaced with a less rigorously defined quantity

$$\sigma'^2_{xx} = 12\pi^5 \int_0^{q_c \lesssim 10/\lambda} q^5\, S(q)\,dq, \tag{5}$$

provided that $\left[2\pi \int_{q_c}^{\infty} q\, S(q)\,dq\right]^{1/2} \ll \lambda$

where the integration is carried out over surface structure of scale greater than about $\lambda/10$. Because parameter μ always increases with λ, every surface will violate the assumptions of a gently undulating model for sufficiently large wavelength unless σ'^2_{xx} decreases at least as rapidly as λ^{-2}.

Quasi-specular scatter will be wavelength independent over any range of wavelengths for which $\mu = \frac{\lambda^2}{2\pi^2}\sigma'^2_{xx}(\lambda')$ is less than about 1, for a fixed λ'. As an example, consider two wavelengths λ_1 and λ_2 with $\lambda_1 > \lambda_2 = \lambda'$. Then if

$$\mu_{2,2} = \frac{\lambda_2^2}{2\pi^2}\,\sigma'^2_{xx}(\lambda_2) \tag{6}$$

and

$$\mu_{1,2} = \frac{\lambda_1^2}{2\pi^2}\,\sigma'^2_{xx}(\lambda_2)$$

are both less than about 1 ($\mu_{1,2}$ will be greater than $\mu_{2,2}$), the surface can be well-approximated by a gently undulating model and there will be no significant wavelength dependence over this range. Stated another way, given $\sigma'^2_{xx}(\lambda_2)$ such that $\mu_{2,2} \lesssim 1$, the upper limit over λ, over which little or no wavelength dependence is expected can be easily found. Surfaces with sharply declining curvature spectra have $\sigma'^2_{xx}(\lambda)$ that rapidly converge to their final value ($\sigma^2_{xx}(\infty)$). These surfaces display constant quasi-specular scatter for all wavelengths less than some critical value. The rapid convergence of σ'^2_{xx} corresponds to a lack of small scale surface structure. Conversely, for a real surface at any wavelength such that $\mu' = \frac{\lambda'^2}{2\pi^2}\,\sigma'^2_{xx}(\lambda') \gtrsim 1$, the assumptions of the gently undulating model are not fulfilled and wavelength variations in the scatter can be expected. However, no general, rigorous analytical method is available to calculate these variations explicitly.

In Paper I we estimated the wavelength dependence of the apparent surface roughness, as sensed by radar, for several examples of power law height variance spectra under the assumption that a fixed value of $\mu = \mu'$ defines an upper bound to the spatial frequencies that contributes to quasi-specular scatter. These results are summarized in Table I and will be referred to below. Note that there is a marked change in the strength of the wavelength dependence for values of the spectral index n between 3 and 4. For larger values of n, σ_x is virtually independent of wavelength. Also, there is only slight change in the power of the wavelength variation, from $-1/2$ to $-1/3$ as the height variance spectrum changes from a constant to an inverse cube law.

Comparison with Height-Variance Spectra

The work described in this section was based on detailed lunar topography as determined by photogrammetry, supplied by H. Moore and his colleagues at the U.S. Geological Survey. Their results are based upon Apollo photographs taken from lunar orbit. Detailed descriptions of the photogrammetric procedures and error sources have been given elsewhere (Moore and Wu, 1973; Wu et al., 1973).

We obtained the data in numerical form as a sequence of planar location coordinates and associated heights. Samples were separated laterally by 25 m, which was the closest spacing for which reliable estimates of slope could be obtained. Typically, the height was given for each of three determinations at each locating coordinate. The dispersion among these repeated samples was used to estimate the statistical sampling error and this error was converted to a value for the spectral noise floor under the assumption that the errors at different locations were uncorrelated. Several hundred to about one thousand samples were available at each sampling site. The sampling locations are arranged in systematic patterns that vary from site to site. A linear sampling traverse was most common, but rectangles, "L"s and zig-zags also occurred. These patterns were chosen to maintain all samples within a similar terrain type, or to avoid a feature that was judged by the geologists to be non-representative of the unit of interest, such as a bright crater ray in otherwise uniform mare material. Uniform area samples from which two-dimensional height-variance spectra can be computed directly were not available.

Since our interest here is in the high frequency behavior of the height-variance spectrum, all data were treated as though they were obtained from a single linear traverse. In the few cases of folded patterns, this procedure distorts the low frequency portions of the height-variance estimate, but is not believed to introduce serious error for our purposes. The height-variance spectra computed from these data are detrended and have

30 degrees of freedom. Typical results are given in Figure 2.

The asymptotic behavior of such spectra was estimated by two methods. Let $\hat{S}(q_x)$ represent a one-dimensional height variance spectrum estimated from the data. It was assumed (on the basis of previous results) that the asymptotic behavior has the form

$$\hat{S}(q_x) = C\, q_x^{-t} \tag{7}$$

The constants C, t were obtained first by least-mean-square fits to log (C) -t log (q_x) between limits $q_{x_{min}}$, $q_{x_{max}}$, which were selected by inspection of plots such as those given in Figure 2. The fitting region was chosen to avoid low frequency turn-overs and, occasionally, erratic fluctuations in the extreme high frequency portions of the spectrum. Typically, $q_{x_{min}}$ = .001 cycle/m, while $q_{x_{max}}$ was chosen as the highest available frequency (.02 cycle/m) unless the estimates of sampling noise and the appearance of the spectrum both indicated a problem at the higher frequencies.

As a check on this procedure we also determined the best linear fit to

$$\log (\hat{S}(q_x) - \hat{N}) \tag{8}$$

where $\hat{N}$ represents the spectrally uniform contribution that would result from uncorrelated photogrammetric reading errors. The value of $\hat{N}$ for which the fitting

error was minimum was taken as an estimate of the noise floor. Corresponding values of $\hat{C}$, $\hat{t}$ were taken to represent the asymptotic behavior of $S(q_x)$. In this case $q_{x_{min}} = .002$ cycles/m and $q_{x_{max}} = .02$ cycles/m. The values $\hat{N}$ and the corresponding estimate obtained from the sampling error generally agree within a factor of about 2.

As a final estimate of C, t the values of the spectral index t obtained by the two methods were averaged. The spread in the two values was used as an estimate of error. Because the constant C was believed to be much better determined than the slope, and the final results are not sensitive to its precise value, only the second determination of this quantity was used.

To be useful in a two-dimensional power-law formulation of the surface roughness, these results must be interpreted in terms of the two-dimensional spectrum

$$S(q) = k\, q^{-p} \tag{9}$$

It is shown in the Appendix that the relationship between the power law spectrum $S(q_x)$ based on one-dimensional sampling and an underlying two-dimensional power-law $S(q)$ is

$$p = t + 1$$

$$k = .1087\, S(q_{xo}) q_{xo}^{t} (t+1)^{.76}, \qquad 2 \lesssim t \lesssim 5 \tag{10}$$

The relations (10) were used to express the spectral estimates $\hat{S}(q_x)$ obtained from the linear fitting procedures discussed above in terms of the two-dimensional parameters k,p.

Table II gives the results for all but one of the sites for which oblique-scatter data are also available. The rejected site gives anomalous results for k,p. Examination of the orbital images shows that the photogrammetric results are contaminated by a fresh crater. Values of the error estimate for p are given in parentheses adjacent to the quantity. The indicators and α and β refer to one case for which only the second estimation procedure was used, and to several cases for which the two estimation procedures yield the same result. Note that the final values for the spectral index generally distribute themselves between 3 and about 4, and cluster near the extremes of this range.

Table II also gives the surface mean-square height, h_o^2, calculated directly from the original height sample data. Since k, p represent only asymptotic behavior, a comparison of the spectrum kq^{-p} and h_o^2 is a measure of the low frequency surface behavior.

For reasons that are discussed in the next section of this paper, it is not expected that the high frequency tails of S(q) will turn upwards, i.e., that p will decrease for frequencies higher than those sampled. If the value of p changes, it is expected to increase, i.e., the spectrum will remain the same or become steeper. Still, to our knowledge there are no data on the height-variance spectrum of the lunar surface at frequencies higher than those shown here, so extrapolation to much smaller scales than those sampled directly is required.

The parameterized asymptotic height spectra can now be used to determine the surface parameters of interest to radar scatter. In particular, we could compute $\sigma_{xx}'^2(\lambda)$ directly, and from it the parameter μ', to determine the consistency of the surfaces sampled with the assumptions of the quasi-specular model. However, for purposes of comparison with radar data it is more convenient to use $S(q)$ to determine the spatial frequency $q_1^*(\lambda)$ at which μ' exceeds some threshold. Redefine $\sigma_{xx}'^2$ in terms of specific values for the upper and lower bounds,

$$\sigma_{xx}'^2 = 12\pi^5 \int_{q_0}^{q_1} q^5 S(q)\, dq \qquad (11)$$

where q_1 is the effective upper bound and q_0 is the effective low frequency cut-off required for a power-law spectrum. Substituting kq^{-p} for $S(q)$,

$$\sigma_{xx}'^2 = \frac{12\pi^5 k}{6-p}\, q_1^{6-p} \left(1 - \left(\frac{q_0}{q_1}\right)^{6-p}\right), \quad p \neq 6 \qquad (12)$$

For our data, q_0 is computed by extrapolating kq^{-p} to low frequencies until the integrated value of the height spectrum is equal to the mean-square height, i.e., by solving

$$h_o^2 = 2\pi \int_{q_o}^{\infty} q' S(q)\, dq$$

for q_o. It is easy to show that the result is insensitive to the upper limit for the spectra $S(q)$, of interest here. Values of q_o are typically 10^{-6} cycles/m, with a maximum value obtained of 3.5×10^{-5} cycles/m for Mare Serenitatis in Table II. Values obtained for q_1 are much larger. Thus, the second term in the expression for $\sigma_{x'x'}^2$ can be neglected, with the result that

$$q_1^* = \left[\frac{(6-p)\sigma_{x'x'}^2}{12\pi^5 K} \right]^{\frac{1}{6-p}}, \quad p < 6 \qquad (13)$$

The asterisk is used to denote the value of q_1 estimated from the data, i.e., for the specific values of k,p obtained from reduced surface height sample data. Referring to Figure 1, we take $\mu' = 1$ as a reasonable upper bound for the conditions under which a real surface can be approximated by a gently undulating model approximation. For this condition about 90 percent of the specular points fulfill the required approximations; for smaller values of μ' the degree of approximation rapidly becomes much better. Further, we take $\cos^4\gamma = .8$ as a typical value for this quantity to account for components of the scatter somewhat removed from the centroid of the scatter.

Then, since

$$\sigma_{xx}'^2 = \frac{2\pi^2 \mu'}{\cos^4\gamma\, \lambda^2}$$

we have

$$\sigma_{xx}'^2(13) = 910 \qquad (14)$$

$$\sigma_{xx}'^2(116) = 12$$

Expression (13) above has been evaluated for the locations of interest using these values of $\sigma_{xx}'^2$ at λ = 13 and 116 cm, the two wavelengths of the Apollo bistatic radar observations; the results for q_1^* are given in Table II.. The range of q_1^* corresponding to the spread in values of p is about a factor of 2; extreme values are given in parentheses for q_1^* (13) only. A similar range of variation will result for q_1^* (116). Typically, the values of q_1^* lie between about 1 and 100. A notable exception occurs at the Apollo 17 landing site, where q_1^* (13) and q_1^* (116) are 550,000 and 11,000, respectively. This particular surface is extremely smooth at small scales.

A second test for consistency between the gently undulating surface and the asymptotic height variance spectrum lies in the value of the calculated mean-square slope σ_x for a particular upper frequency bound, q_1, determined by the curvature. Again, it is more convenient to compare the bounds for a particular case. It is easy to show that

$$\hat{q}_1 = \left(\frac{6-p}{4-p} \cdot \frac{1}{3}\right)^{1/2} \frac{1}{\pi} \frac{\sigma_{xx}}{\sigma_x}$$

$$p < 4 \qquad (15)$$

$$\hat{k}_1 = \frac{4-p}{4\pi^3} \frac{\sigma_x^2}{\hat{q}_1 (4-p)}$$

where the hat denotes the simultaneous solution with respect to curvature, σ_{xx}, and slope, σ_x. That is, for a particular spectral index p, $\hat{q}_1$ and $\hat{k}_1$ are the bound and constant that result in particular values of σ_{xx} and σ_x. The quantities $\hat{q}_1$, $\hat{k}_1$ have been evaluated and are given also in Table II for particular values $\sigma_{xx} = 12$, corresponding to $\mu' = 1$, $\lambda = 116$ cm, and $\sigma_x^2 = 0.02$, which represents a typical lunar highland surface tilt of 11° rms.

Values of $\hat{q}_1$, $\hat{k}_1$ for other choices of these parameters can be easily obtained from those tabulated in Table II and the formulas above.

The criteria for wavelength independence developed above under "Requirements for Radar Model" can be applied to the q_1^* (116). According to our previous discussion, no wavelength dependence is expected for quasi-specular scatter if $\mu_{1,2} \lesssim 1$, or what is equivalent, if q_1^* (116) $\gtrsim$ 8 cycles/m. That is, that the surface characterized to scales of 13 cm must also be gently undulating on the scale of 116 cm. This criterion is clearly satisfied by the surfaces at four locations in Table II and violated at seven others. There is one borderline case, Descartes. Generally, these surfaces are separated into two categories for which q_1^* (116) $\sim$ 2 and q_1^* (116) $\sim$ 10.

This separation is stronger when values of k, $\hat{k}_1$ and q_1^* (116), q_1^* are compared. Those surfaces for which $\mu' \lesssim 1$ are also those for

which the $\hat{k}_1$, $\hat{q}_1$ required to bring the slopes and curvature simultaneously into agreement are near the k, q_1^* (116) derived from the surface height data. For these sites $k \sim \hat{k}_1$, although the $\hat{k}_1$ are systematically too small by a factor of about 2, while q_1^* (116) $\sim \hat{q}_1$, but the $\hat{q}_1$ may be systematically too large. These small systematic disagreements are not surprising. There are large differences between these pairs of values for the other locations. This is particularly evident in the differences between k and $\hat{k}_1$, where k typically exceeds $\hat{k}_1$ by an order of magnitude or more. Most of the sites in this second category are in areas of low to moderate slopes. The discrepancies would be considerably larger if smaller values of σ_x corresponding to the observed slopes for these locations had been used to estimate $\hat{q}_1$, $\hat{k}$ rather than the value $\sigma_x^2 = .02$ actually used. Descartes apparently should be included with the first group of sites.

Finally, Table II also includes values of rms slope obtained from scatter observations with Apollos 14 and 15. In simplest terms, the values $\sigma_x(\cdot)$ given are direct measures of the angular one-half power width of the obliquely scattered echo, corrected for certain geometrical factors, and reduced to a unidirectional rms slope on the basis of a gently undulating surface model. The parameter, 13 or 116, indicates the wavelength of observation in cm. Complete descriptions of this experiment, the underlying theory, and the data reduction process have been given elsewhere (Tyler and Howard, 1973; Tyler et al., 1973).

Some further comments are needed for several of the sites. There are no radar data of this type for the Apollo 17 landing site; this site was included in the table only as an example of an extremely smooth surface sampled by photogrammetry. There are two sites for which

no radar data were directly available, but where geologic maps (Eggleton, 1965; Howard and Masursky, 1968) indicate that the radar has sampled the same unit within a short distance of the photogrammetric traverse.. These sites are Cratered Terrain and Mare Cognitum. Mare Cognitum is a large, uniform area with little complexity. Cratered Terrain is embedded in highland materials. One location, Cayley, is included although radar data are given only for λ = 13 cm. This unit is included because it was observed directly by Apollo 16. However, there were severe experimental problems with the 116 cm wavelength data from the Apollo 16 experiment, so that no reliable results are available for $\sigma_x(116)$. The Apollo 16 data show no significant change in the scatter at either 13 or 116 cm wavelength between the Cayley unit which is located in the crater Ptolemaeus and the highlands material surrounding it. Since highlands units observed with both Apollos 14 and 15 generally display wavelength independent scatter, this Apollo 15 observation is taken as evidence that the scatter from Cayley is also wavelength independent. Further, the values of $\sigma_x(13)$ for Apollo 16 are known to be systematically low with respect to those of Apollos 14 and 15, but the cause of this problem is not known.

All locations for which the photogrametrically sampled surface is apparently consistent with the gently undulating surface display wavelength independent quasi-specular scatter, as expected. Of the other locations, only Cratered Terrain and Mare Undarium fail to show a strong wavelength dependence, although a weak variation is present. The remaining sites typically have a 1.5 to 2.0 to 1 variation in σ_x between 13 and 116 cm wavelength. On the basis of our previous work, a 2 to 1 variation

would be expected over this range for an inverse cube law dependence in $S(q)$ (v. Table I).

These results show a general quantitative agreement between the onset of wavelength dependence in radar observations and the consistency of the surface with the radar model as determined from independently measured surface height statisics. If the assumption that the variance spectrum of the lunar surface only becomes steeper at smaller scales is correct, then the unexpectedly weak variations in σ_x at Mare Undarum and Cratered Terrain locations can be explained also.

Unfortunately, Table II exhausts the available sets of co-located lunar topographic data and radar observations. There are no appropriate lunar surface data of this type other than those considered here.

Comparison with D_L Values

One of the more striking characteristics of the lunar surface is the ubiquity of craters and the absence in orbital photographs below a scale of about 1 km of any apparent change in the distribution of the crater population. This latter characteristic was predicted by Moore (1964) and others (Shoemaker, 1965). It is generally believed to result from a saturation bombardment of the surface by meteorites, to the level where old carters are destroyed as fast as new ones are created. The size of the largest crater that belongs to this steady population increases with time. Craters larger than this limiting size have a distinctly different distribution whose origin is not well understood.

The size-frequency distribution of lunar craters can be determined from photographs. Figure 3 gives a schematic illustration of the cummulative crater population for a typical surface. The ξ^{-2} region represents the steady state condition, while the ξ^{-3} is typical for craters greater than a particular size, called C_S. For sizes greater than about 1 km, there is a second break to a third slope which is not of interest here.

Lunar crater size-frequency distributions have been studied extensively, and are well represented by the curves just described (v., e.g., Soderblom and Lebofsky, 1972; Gault, 1970). As indicated C_S increases with time, and the breaking point moves along the extrapolated ξ^{-2} line. The underlying theory for interpretation of these distributions has been confirmed by numerical modeling and experimentally in the laboratory so that the functional form is well established. Of considerable importance here, the ξ^{-2} portion of the distribution

has been verified to scales at least as small as 10 cm by in-situ observations of the lunar surface (Morris and Shoemaker, 1970). This observation is thought to be representative of plains surfaces on the moon, but may break down in extremely rough areas where other mechanisms, such as downslope transport, also modify the surface at small scales (H. J. Moore, private communication, 1977). Because a determination of C_S requires careful counting of craters, a second measure of surface age based on recognition of the eroded morphology of large craters has been developed (Soderblom and Lebofsky, 1977). This measure is D_L, which is defined as the diameter of the largest crater that has eroded to an internal slope of 1°. The quantity D_L is readily determined from lunar photographs by identification and measurement of certain craters with a particular shadow geometry, with a simple correction for sun angle. Values of D_L are available for most of the Apollo 14 and 15 oblique-scatter data from plains units (Moore et al., 1975, 1976). The quantities D_L and C_S are in approximately constant ratio, $D_L = 1.7\ C_S$ (H. J. Moore, private communication, 1977). Because of the simple relationship between D_L and the size-frequency distribution, it is easy to derive an approximate relationship between D_L and the form of the height-variance spectrum.

We assume that all craters of the same size give rise to the same spectral contributions to the overall height-variance spectrum, i.e., that on the average the height-variance spectra of individual craters of the same size are the same, and that the spectra of individual craters scale in accordance with the variation of a crater of variable size but fixed shape. Within the steady-state fraction of the distribution this is clearly not the case, because craters of any particular size are found in all stages of erosion. However, this factor will tend to smooth the small scale surface more rapidly than would be the case under our assumption.

Let $f(\rho)$ be an assumed crater profile, where ρ is the radial coordinate, then the crater scales as $af(\rho/a)$ if both vertical and horizontal dimensions increase by the same factor a. The Hankel transform of $f(\rho)$ is

$$H[f(\rho)] = s(q) = 2\pi \int_0^\infty \rho\, f(\rho)\, J_0(2\pi\rho q)\, d\rho \qquad (16)$$

from which it is easy to show that

$$H[a\, f(\rho/a)] = a^3\, s(aq) \qquad (17)$$

The two-dimensional height variance spectrum, $\bar{S}(q) = |s(q)|^2$, then goes as $a^6\, \bar{S}(aq)$, where the bar denotes the spectrum of an individual crater. Therefore, for a crater of size ξ, the individual contribution to the spectrum scales as $\xi^6\, \bar{S}(\xi q)$ relative to the spectrum of an individual crater of size unity.

If all craters are statistically independent, then the spectrum for the total surface is

$$\tilde{S}(q) = \int_0^\infty p(\xi)\, \xi^6\, \bar{S}(\xi q)\, d\xi \qquad (18)$$

where $p(\xi)$ is the marginal probability density function per unit area that a crater of size $\xi, \xi+d\xi$ is present. This simple form results from the assumption of statistical independence, so that the

spectra of the individual craters add incoherently. Other assumptions regarding the relationships among the various individual craters or other scaling laws lead to drastically more complex forms. This topic deserves further investigation.

Describe the cumulative size-frequency distribution as

$$\hat{P}(\xi) = a \qquad \xi < D_0$$

$$= \frac{a\, D_0^2}{\xi^2} \qquad D_0 < \xi < D_L' = C_S = D_L/1.7 \tag{19}$$

$$= \frac{a\, D_0^2\, D_L'}{\xi^3} \qquad D_L' < \xi$$

Where D_L' is introduced as a convenience. Then, the marginal density function is

$$p(\xi) = \frac{d}{d\xi}\left(1-\hat{P}(\xi)\right) = 0 \qquad \xi < D_0$$

$$= \frac{2a\, D_0^2}{\xi^3} \qquad D_0 < \xi < D_L' \tag{20}$$

$$= \frac{3a\, D_0^2\, D_L'}{\xi^4} \qquad D_L' < \xi$$

For this model $a=1$, so D_o must be interpreted as the size of the smallest crater.

We also assume a power law for $\bar{S}(q)$

$$\bar{S}(q) = b, \qquad q < q_b$$

$$= b(q_b/q)^{\nu}, \quad q_b \le q \tag{21}$$

$$\bar{S}(\xi q) = b, \qquad \xi q < q_b$$

$$= b\left(\frac{q_b}{\xi q}\right)^{\nu}, \quad q_b \le \xi q$$

The frequency q_b/ξ here plays the role of a cutoff for the spectrum of the individual crater. Substituting in (17) to find the surface spectrum

$$\begin{aligned}\tilde{S}(q) = {} & C_1 \cdot \int_{D_o}^{\mathrm{Min}(D_L', q_b/q)} b\xi^3 \, d\xi + C_1 \cdot \int_{\mathrm{Min}(D_L', q_b/q)}^{D_L'} b\, \xi^{3-\nu}(q_b/q)^2 \, d\xi \\ & + C_2 \cdot \int_{D_L'}^{\mathrm{Max}(D_L', q_b/q)} b\, \xi^2 \, d\xi + C_2 \cdot \int_{\mathrm{Max}(D_L', q_b/q)}^{\infty} b\, \xi^{2-\nu} \, (q_b/q)^{\nu} \, d\xi\end{aligned} \tag{22}$$

Where $C_1 = 2\ D_o^2$, and $C_2 = 3\ D_o^2\ D_L'$. Clearly only three of these terms can be non-zero at any one time; which three depends on the relative sizes of D_L' and q_b/q. Evaluating the integrals,

$$\frac{\tilde{S}(q)}{b} = \frac{C_1}{4}\left\{(q_b/q)^4 - (D_o)^4\right\} + \frac{C_1}{4-\nu}(q_b/q)^\nu\left\{(D_L')^{4-\nu} - (q_b/q)^{4-\nu}\right\}$$

$$+ \frac{C_2}{3-\nu}(q_b/q)^\nu\left\{\lim_{\xi\to\infty}\ \xi^{3-\nu} - (D_2')^{3-\nu}\right\}, \qquad \frac{q_b}{D_L'} < q$$

$$\nu \neq 3,4 \tag{23}$$

$$= \frac{C_1}{4}\left\{(D_L')^4 - (D_o)^4 + \frac{C_2}{3}\ (q_b/q)^3 - (D_L')^3\right\}$$

$$+ \frac{C_2}{3-\nu}\ (q_b/q)^\nu\left\{\lim_{\xi\to\infty}(\xi^{3-\nu}) - (q_b/q)^{3-\nu}\right\}, \qquad \frac{q_b}{D_L'} > q$$

$$\nu \neq 3,4$$

For $\nu > 4$,

$$\tilde{S}(q) \rightarrow q^{-3}, \quad q < q_b/D_L'$$

$$\rightarrow q^{-4}, \quad q > q_b/D_L'$$

For large values of ν, for which $\bar{S}(q)$ is approximated by

$$\bar{S}(q) = b, \quad q < q_b$$

$$= 0, \quad q_b \leq q$$

a more simple form is obtained,

$$\tilde{S}(q) = \frac{C_1}{4} D_L'^4 \left(1 - \left(\frac{D_o}{D_L'}\right)^4\right) + \frac{C_2}{3} D_L'^3 \left\{\left(\frac{q_b}{D_L' q}\right)^3 - 1\right\}, \quad q < \frac{q_b}{D_L'} \qquad (24)$$

$$= \frac{C_1}{4} D_L'^4 \left(\left(\frac{q_b}{D_L q}\right)^4 - \left(\frac{D_o}{D_L'}\right)^4\right), \quad \frac{q_b}{D_L'} \leq q$$

Clearly, for all cases for which $\tilde{S}(q)$ unconditionally converges i.e., $\nu > 4$, $\tilde{S}(q)$ is of the form of a two-segment power law with indices 3,4 over most of the range of spatial frequency q. This characteristic arises from the form of the crater size-frequency distribution (i.e., ξ^{-2}, ξ^{-3}) and the edge, or break in $\bar{S}(q)$. The simplified result corresponding to large values of ν is plotted in Figure 4.

The critical parameter in this result is the ratio of the break frequency q_b to D_L'. There are no data on the variance spectra of individual lunar craters (H.J. Moore, private communication, 1977). But, a small nuclear test crater, "Danny Boy", has been sampled adequately to demonstrate significant roughness to spatial frequencies that extend to many times the inverse crater diameter (Moore et al., 1974). This characteristic is also readily apparent in images. Examination

of lunar images suggests that fresh craters have significant roughness to perhaps 100 times the inverse crater diameter (v. e.g. Moore, 1971). It is clear from experiments that the details of a particular cratering event, especially the nature of the target material, are of paramount importance in this regard (v. e.g. Oberbeck, 1975).

For our normalized spectrum $S(q)$, the value of the break point q_b is just the highest signficant frequency measured in inverse diameters. Typical values for D_L' in lunar plains units range between about 100 and 500. If the model for $S(q)$ proposed here is approximately correct, then the break point for the spectrum will occur for $q \sim 1$. This value is of the same order as the inverse of the radar wavelengths, λ^{-1}, for the scatter data considered here.

Note that the high frequency, $\sim q^{-4}$, portion of $\tilde{S}(q)$ is controlled by the saturated, or steady state, region of the crater size-frequency distribution, while the low frequency segment, $\sim q^{-3}$, arises from the craters of size greater than C_S. This occurs because the ξ^{-2} law observed in the steady state represents relatively fewer small craters with respect to the total population than does the ξ^{-3} segment of the size-frequency distribution. The simplified spectrum for the cutoff $\bar{S}(q)$ goes to zero at $q = q_b/D_o$, which represents the highest frequency present in the crater population. Just below this maximum frequency, $\tilde{S}(q)$ falls even more rapidly than q^{-4}. The mixture of crater ages in the steady state distribution will reduce the roughness of an average crater of a particular size relative to the scaled roughness of a crater in the ξ^{-3} population, so that q_b should not be constant for the two portions of the population. The principal effect of this smoothing would be to displace the knee of $\tilde{S}(q)$ towards smaller q.

As shown in Table I, we have previously estimated that $S(q) \sim q^{-3}$ gives rise to $\lambda^{-1/3}$ variation in $\sigma_x(\lambda)$, while $S(q) \sim q^{-4}$ leads to $[\ell n(\lambda)]^{1/2}$, or a very weak wavelength dependence. Hence, radar scatter from surfaces of varying D_L should display a variation in $\sigma_x(\lambda)$ between these two limits, or possibly between $\lambda^{-1/3}$ and λ^0, as the changing q_b/D_L' places the observing wavelengths on different portions of the $\tilde{S}(q)$ curve.

Radar scatter and D_L are compared in Figure 5, where results for Apollos 14 and 15 are given separately. For each plot, the ratio of the rms surface roughness observed at the two Apollo bistatic-radar wavelengths, $\rho = \sigma_x(116)/\sigma_x(13)$, is plotted vs D_L obtained from Apollo and Lunar Orbiter photography. The D_L values used are a slightly revised set of those previously published by Moore et al. (1975, 1976), based on more recent work. The data are restricted to lunar plains units. Each point represents an average value of D_L and σ_x over about 1° of surface arc along the bistatic radar track on the lunar surface. A large area sample is required for reliable estimates of D_L. In most cases there is very little or no variation in σ_x within these areas. There is a clear systematic difference in the Apollo 14 and 15 results (Moore et al., 1976). This difference has been corrected here by multiplication of the Apollo 15 σ_x ratio by 1.22.

The Apollo 14 data show a clear, strong trend in ρ for D_L between about 150 and 400 m; the Apollo 15 data show a similar result over the same range of D_L values, but the relationship between ρ and D_L is much more scattered even though the formal errors in the data are about the same. Both data sets show $\rho \sim .5$ for $D_L \sim 150$ m, and both data sets contain points for $D_L > 400$ m where $\rho \sim 1$. There is a clear variation of ρ with D_L,

most of which occurs over the range $100 \lesssim D_L < 400$m. Further, the variation is of the correct sense with D_L, and the minimum observed value of $\rho \sim .5$ is approximately the correct value ($\xi^{-3} \rightarrow \lambda^{-1/3}$, $(13/116)^{1/3} \doteq .48$), to be explained by a variation in S(q) of the type modeled here. In the Apollo 14 data, the minimum value of the ratio is $\rho = .40$, for Apollo 15 the minimum value is $\rho = .46$ (or $.46/1.22 = .38$ before scale factor correction). This seems to be in good agreement with $\lambda^{-1/3}$ when it is remembered that these values of ρ are noisy.

Linear regression was used to obtain an objective measure of the variation of ρ with D_L. Other functional forms were also tried, but the data were not thought to warrant much more elaborate treatment. A D_L value of 400m was selected as an upper bound to the fitting region on the basis of the Apollo 14 data, which have an apparent knee at about that point. The results are given in Table III for several combinations of data.

The two cases labelled Apollo 14 and Apollo 15 are the individual results for the complete data sets from those experiments for $D_L < 400$ m. The increased noisiness of the Apollo 15 results appears in the much lower regression coefficient, r^2, calculated for that case. Deleting the three points farthest from the regression line, the case labelled Apollo 15, except 3 points, increases the regression coefficient by a factor of 1.6. The fourth case, labelled Apollo 14 and Apollo 15, includes all data points and represents a reasonable fit of the regression line.

The origin of the systematic differences between the Apollo 14 and Apollo 15 data is not known. These differences are apparent in the radar data alone (cf. Apollo 14 and Apollo 15 results in Moore et al, 1975, 1976). They may be related to a change in the experimental conditions, specifically the spacecraft antenna configuration, between the two sets of observations, or they may reflect real systematic differences between the Maria Serentitates and Imbrium, the primary source of Apollo 15 data, and the Oceanus Procellarum, the primary source of the Apollo 14 data. A third possibility lies in the sources of the images that were used to determine D_L. The Apollo 14 D_L values are based almost entirely on Lunar Orbiter results, while Apollo 15 D_L values are based on those from Apollo (Moore et al, 1975, 1976). Regardless of the differences, both sets of data display the same behavior, and the results from the combined set, Apollo 14 and Apollo 15, are taken as the best estimate of the variation, even though the regression coefficient is higher than for the Apollo 14 case alone. The changing wavelength dependence of radar scatter with lunar surface characteristics has also been presented elsewhere in forms that are readily compared with images and maps (Tyler and Howard, 1973; Howard and Tyler, 1972; Moore et al., 1975, 1976).

Conclusions and Remarks

The wavelength dependence of quasi-specular scatter is readily measured but has not been well understood. Scatter from most of equatorial Mars shows essentially no variation in the apparent surface roughness over wavelengths from a few centimeters to meters. Similar scatter from the moon shows little or no variation over the same wavelength range in highland areas, but does have an approximately 2:1 variation in most mare areas. It is believed that these differences in scatter are related to differences in surface roughness on approximately wavelength-sized scales, but almost no quantitative work has been carried out. Paper I suggested a quantitative procedure to estimate wavelength dependence in terms of small scale surface roughness as expressed through the height variance spectrum.

This work has been an attempt (1) to test the consistency of the gently undulating surface model for radar scatter and the natural lunar surface -- which has not been done before -- and to compare the results with observed scattering behavior, and (2) to verify the previous estimates of wavelength dependence given in Paper I.

The circumstantial evidence for the dependence of the apparent roughness $\sigma_x(\lambda)$ on the height variance spectrum $S(q)$ is strong. Expected radar characteristics based on estimates of the height variance spectrum are in good agreement with observations of radar scatter at the same locations. These comparisons suffer from the need to extrapolate to small roughness scales; but, it was also shown that $S(q) \propto q^{-4}$ is the expected form for the high frequency portions of the variance spectrum. On this basis, extrapolation of $S(q)$ with

index p near 4 would be accurate. For smaller values of p, the spectrum might soften, but is not expected to turn upwards. The results are consistent with this model. There are examples of strong wavelength dependence,and others where there is little or no variation with wavelength. Values of D_L, the diameter of a crater eroded to 1° internal slope, are clearly related to variations in radar roughness with wavelength. The comparison of radar scatter with D_L values is completely dependent on the model for surface aging as a link to S(q). While this model is well established, the calculation of S(q) from that model is not rigorous. But a reasonable choice for the free parameter q_b also leads to approximate quantitative agreement between the observed radar behavior and its variation with D_L. Further work is needed on this problem. The realization that D_L can be directly related to surface roughness on much smaller scales is apparently new.

Two different approaches to the data, one based on detailed samples at a single location, but limited in surface resolution to about 25 m, and a second based on the statistical morphology of lunar craters over much larger areas, but which uses a surface aging model valid to scales at least as small as 10 cm, give similar results. Prior to this, there has been no demonstration that either the magnitude or approximate asymptotic shape of S(q) would yield values of σ_x^2, σ_{xx}^2, and μ that were compatable with the gently undulating model, or the filtered surface model for wavelength dependence. Neither has there been any model which predicted the variation in wavelength dependence with D_L, based on the changing position of the knee in $\tilde{S}(q)$. Better understanding of this problem will require a new body of data from which radar scattering can be compared with surface statistics based on detailed measurements at sub-wavelength scales.

Appendix

Consider a statistically isotropic two-dimensional surface described by a power spectrum.

$$S(q) = \int_0^\infty R(\tau)\, \tau\, J_0\, (2\pi\tau q)\, d\tau$$

where $R(\tau)$ is the auto-correlation function and $S(q)$ is assumed to be asymptotically

$$S(q) = K\, q^{-p},\ q_1 < q$$

i.e., to follow a power law for q sufficiently large. Then the one-dimensional spectrum associated with a profile of the two-dimensional along any fixed direction is

$$S(q_x) = \int_{-\infty}^{+\infty} S\left(\sqrt{q_x^2 + q_y^2}\right) dq_y,\ q_1 < q_x$$

where $q^2 = q_x^2 + q_y^2$, and we have aligned the sampling direction with q_x. Evaluating this expression

$$S(q_x) = \frac{2\,k}{\cdot q_x^{p-1}} \int_0^\infty \frac{d_{qy}}{(1+q_y^2)^{p/2}}$$

so that if $S(q)$ is power law, $S(q_x)$ is also with spectral index reduced by 1. The integral

$$\int_0^\infty \frac{d_{qy}}{(1+q_y^2)^{p/2}}$$

is approximated by $2.30\ p^{-.76}$ to less than 2% error, over a small range in p, $3 < p < 6$.

These results lead directly to the forms given in expressions (10) of the text.

Acknowledgment

The author wishes to acknowledge the work of A. Chu in reduction of the height variance spectra to the forms used here, and to express his special appreciation to H. J. Moore for many helpful comments and criticisms. This work was supported by the National Aeronautics and Space Administration under Grant NGR 7029.

References

Barrick, D. E. (1968), Rough surface scattering based on specular point theory, IEEE Trans. Antennas Propagat. AP-16, 449-454.

Barrick, D. E. (1970), Rough surfaces, chap 9 in Radar Cross Section Handbook, edited by G. T. Ruck, 949 pp., Plenum, New York.

Beckmann, P. A. (1963), Part I of The Scattering of Electromagnetic Waves from Rough Surfaces, by P. A. Beckmann and A. Spizzichino, 503 pp., Pergamon, New York.

Downs, G. S., P. E. Reichley, R. R. Green (1975), Radar measurements of Martian topography and surface properties: The 1971 and 1973 oppositions, Icarus, 26, 273-312.

Downs, G. S., R. R. Green, and P. E. Reichley (1978), Radar studies of the Martian surface at centimeter wavelengths: the 1975 opposition, Icarus, in press.

Eggleton, R. E. (1965), Geologic map of the Riphaeus Mountains region of the Moon, USGS Miscellaneous Geol. Inv. Map I-458 (LAC 76).

Evans, J. V. (1969), Radar studies of planetary surfaces, in Ann. Rev. Astron. Astrophys., 7, 201-248.

Gault, D. E. (1970), Saturation and equilibrium conditions for impact cratering on the lunar surface: Criteria and implications, Radio Science, 5, 273-291.

Hagfors, T. (1966), The relationship of geometric optics and auto-correlation approaches to the analysis of lunar and planetary data, J. Geophys. Res., 71, 379-383.

Howard, H. T., and G. L. Tyler (1972), Bistatic radar investigations, Apollo 15 Preliminary Science Report, NASA SP-289, p. 23-1.

Howard, K. A., and H. Masursky (1968), Geologic map of the Ptolemaeus quadrangle of the moon: USGS Miscellaneous Geol. Inv. Map I-566 (LAC 77, RLC-13).

Moore, H. J. (1964), Density of small craters on the lunar surface, in Astrogeologic studies, ann. prog. report, August 24, 1962 - July 1, 1963, D. USGS., (Openfile report), 34-51.

Moore, H. J. (1971), Geologic interpretation of lunar data, Earth-Sci. Rev., 7, 5-33.

Moore, H. J., R. V. Lugn, and E. B. Newman (1974), Some morphometric properties of experimentally cratered surfaces, Jour. Res. U.S.Geo. Survey, 2, 279-288.

Moore, H. J., G. L. Tyler, J. M. Boyce, R. W. Shorthill, T. W. Thompson, A. S. Walker, D. E. Wilhelms, S. S. C. Wu, and S. H. Zisk (1975), Correlation of photogeology and remote sensing data along the Apollo 14 bistatic-radar ground track, Part I - a working compendium, USGS Interagency Report: Astrogeology 75, (open file report 75-284).

Moore, H. J., G. L. Tyler, J. M. Boyce, R. W. Shorthill, T. W. Thompson, D. E. Wilhelms, S. S. C. Wu, and S. H. Zisk (1976), Correlation of photogeology and remote sensing data along the Apollo 14, 15, and 16 bistatic-radar ground tracks, Part II - a working compendium, USGS Interagency Report: Astrogeology 80, (Open file report 76-298).

Moore, H. J., and S. S. C. Wu, (1973), Effect of photogrammetric reading error on slope frequency distributions (Part C, Remote sensing and photogrammetric studies, Appendix), NASA SP-330, Apollo 17 Prelminary Science Report, U.S. Gov. Printing Office, Washington D.C., 33/26 - 33/34.

Morris, E. C. and E. M. Shoemaker (1970), Geology: Craters, Icarus, 12, 167-172.

Oberbeck, V. R. (1975), The role of ballistic erosion and sedimentation in lunar stratigraphy, Rev. Geophys. Space Phys., 13, 337-362.

Shoemaker, E. M. (1965), Preliminary analysis of the fine structure in Mare Cognitum, in Ranger VII, pt. II - Experimenters' Analyses and Interpretations, Calif. Inst. of Technology, Jet Propulsion Lab., Technical Report 32-700, 75-134.

Simpson, R. A., G. L. Tyler, and B. J. Lipa (1977), Mars surface properties observed by Earth-based radar at 70-, 12.5-, and 3.8 cm wavelengths, Icarus, 32, 147-167.

Soderblom, C. A., and L. A. Lebofsky (1972), Technique for rapid determination of relative ages of lunar areas from orbital photography, J. Geophys. Res., 77, 279-296.

Tyler, G. L. (1976), Wavelength dependence in radio-wave scattering and specular-point theory, Radio Science, 11, 2, 83-91.

Tyler, G. L., and H. T. Howard (1973), Dual-frequency bistatic-radar investigations of the moon with Apollos 14 and 15, J. Geophys. Res., 78, 4852-4874.

Tyler, G. L., H. T. Howard, and G. R. Dow (1973), Stanford Apollo bistatic-radar experiment (S-170): National Space Science Data Center Data Description, Stanford Univ., Stanford Elect. Lab. Technical Report 3282-1.

Wu, S. S. C., F. J. Schafer, G. M. Nakata, R. Jordan, (1973), Respectability of elevation measurements - Apollo Photography (Remote sensing and photogrammetric studies, Part D), NASA SP-330, Apollo 17 Preliminary Science Report, U.S. Gov. Printing Office, Washington D.C., 33/35 - 33/34.

TABLE I. ASYMPTOTIC WAVELENGTH DEPENDENCE
FOR POWER LAW SPECTRA

n	σ_x (
0	$\sim \lambda^{-\frac{1}{2}}$
3	$\sim \lambda^{-\frac{1}{3}}$
4	$\sim [\text{const.} - \ell n(\lambda)]^{\frac{1}{2}}$
$S(q) =$	$a,\ 0 \le q \le q_1$ $aq_1^n q^{-n},\ q_1 < q$

Tyler, "Comparison of..."

TABLE II. COMPARISON OF PHOTOGRAMMETRICALLY DERIVED SURFACE PARAMETERS AND RADAR ROUGHNESS

LONG	LAT.	NAME	$h_o^2(m^2)$	k	p	q_1*(13)	q_1*(116)	$\hat{q}_1$	$\hat{k}$(.02)	σ_x(13)	σ_x(116)	q_o	PHOTO ID	S/C SOURCE FOR σ_x	
51°15'E	11°40'N	Mare Undarum	100,000	$4.0\times10^{-3}\binom{2.4}{6.6}$	3.0(±.1)	$5.7\binom{7.2}{4.6}$	1.4	$10\binom{10}{9\ 8}$	$1.6\times10^{-6}\binom{1.8}{1.4}$	5.5°	4.5°	$2\ 5\times10^{-7}$	9489 9484	A-15	5
30°46'E	20°10'N	A-17 Landing Site	110	1.3×10^{-7}	4.9(± 1)	5.5×10^{5}	1.1×10^{4}	- γ	-	-	-	2.6×10^{-9}	2755 2750	A-15	21
30°40'E	20°15'N	West of A-17	70	3.4×10^{-5}	3.9(β)	99	13	27	1.2×10^{-5}	5°	5°	1.6×10^{-6}	2755 2750	A-15	25
28°05'E	20°00'N	Mare Serenitatis	1100	$6.1\times10^{-3}\binom{1.3}{28}$	3 0(±.3)	$5\ 0\binom{10}{2.8}$	1.2	$10\binom{11}{9.3}$	$1.6\times10^{-5}\binom{2\ 1}{1.2}$	4°	2°	3.5×10^{-5}	9565 9560	A-15	3
27°30'E	20°10'N	Mare Serenitatis	1100	$9.2\times10^{-4}\binom{1.2}{69}$	3.2(±.4)	$11\binom{35}{4.4}$	2.3	$11\binom{14}{9.5}$	$1.9\times10^{-5}\binom{2.2}{1.3}$	4°	2°	4.4×10^{-6}	9567 9562	A-15	2
24°25'E	10°40'S	Northwest Flank of Theophilus	650	4.3×10^{-4}	3.5(α)	18	3.2	13	2.2×10^{-5}	8°	5°	2.8×10^{-6}	10506 10504(#6)	A-14	15
22°30'E	10°20'S	Kant Plateau	1400	$4.3\times10^{-3}\binom{1.6}{12}$	3.0 (±.2)	$5\ 6\binom{8.8}{3.7}$	1.3	$10\binom{11}{9.5}$	1.6×10^{-5}	7°	5°	1.9×10^{-5}	10544 10542(#7)	A-14	16
18°25'E	9°30'S	South of Zollner	340	3.1×10^{-5}	3.7(β)	71	11	16	2.1×10^{-5}	7°	7°	3.4×10^{-7}	10624 10622(#8)	A-14	17
15°30'E	8°55'S	Descartes	1600	$5.9\times10^{-5}\binom{2.1}{16}$	3 6(±.2)	$47\binom{100}{24}$	7.7	$14\binom{19}{12}$	2.2×10^{-5}	7°	7°	1.4×10^{-7}	4563 4558	A-14	20
2°05'E	9°10'S	Cratered Terrain	14,000	7.2×10^{-4}	3.0(β)	10	2 4	10	1.6×10^{-5}	7° δ	6° δ	3.2×10^{-7}	4649 4644	A-14	11
0°40'W	9°10'S	Cayley	90	2.2×10^{-5}	3.8(β)	99	14	19	1.8×10^{-5}	(4°) ε	-	8.7×10^{-7}	4657 4652	A-16	8
24°25'W	10°20'S	Mare Cognitum	270	$1.1\times10^{-4}\binom{.25}{5.2}$	3.5(±.3)	$31\binom{94}{13}$ cycles/m	5.5	$13\binom{19}{11}$	2.2×10^{-5}	4° ι	2°	1.8×10^{-6}	5445 5440	A-14	7

α Only a single spectral index estimate available.

β Two spectral index estimates agree to two significant figures

γ This result is given as an example of a surface that is extremely smooth on a small scale. Values are not compared with radar because of limited region to which they apply.

δ Radar data from Apollo 14 at 2°30'E, 6°S, similar terrain.

ε Radar data from Apollo 16, 116 cm not used - values known to be in error.

Cayley material in Ptolemaeus, Apollo 16 13 cm shows no significant change from heavily cratered material outside crater (USGS IA #80).

ι Radar data from Apollo 14 at 24°W, 8°S from same map unit (IPM) as photogrammetric data.

TABLE III. REGRESSION ANALYSIS OF $\rho(D_L)$

$\rho = a + bD_L$, $100 \lesssim D_L < 400m$

Case	a	b	r^2	no. pts.
Apollo 14	0.06	0.0027	0.87	14
Apollo 15	0.32	0.0013	0.28	23
Apollo 15, except 3 points	0.29	0.0015	0.44	20
Apollo 14 and Apollo 15	0.17	0.0021	0.57	37

Tyler, "Comparison of..."

Figure Captions

1. Probability that the magnitude of the product of the principal radii of curvature $|r_{12}^2|$ is less than $\hat{r}_{12}^2$. The parameter $\mu = 2\sigma_{xx}^2 r_{12}^2 \cos^4\gamma$ (see text).

2. Sample one-dimensional height variance spectra from lunar photogrammetric data. A. Data from Kant Plateau. B. Data from Cayley (see text, Table II for coordinates, parameters). Light lines are fits to curves according to expression (8) in text. The noise level for both curves is estimated to be 17 m^2/cycle/m ±10, under the assumption that the errors in the photogrammetric samples are uncorrelated. The flattening of curve B for $q_x \gtrsim 10^{-2}$ is believed due to noise from sampling errors. Neither curve is reliable for q_x significantly less than 10^{-3}, due to the detrending procedures.

3. Crater size-frequency distribution model for the lunar surface. Two segments of the distribution follow power laws with indices -2, -3, and break point crater diameter C_S. (This figure adopted from Moore, H. J., J. M. Boyce, and D. E. Meyer, "Lunar Impact Cratering in Recent Times, unpublished, 1977.)

4. Height variance spectrum of model cratered surface. $\tilde{S}(\eta)$ calculated from expression (23) in the text. Discontinuity in slope at $\eta = 1$ is real. Light lines give asymptotes, slopes are -3, -4.

5. Comparison of surface rms slopes inferred from radar at 13 and 116 cm wavelength with D_L, the diameter of the largest crater eroded to a 1° internal slope. Data are from the lunar plains units only. Light lines give the results of fits to data for D_L < 400 m

Figure Captions (cont.)

(see text, cf. Table III). Errors for D_L are numerical average of formal errors for individual data points; errors in $\sigma_x(116)/\sigma_x(13)$ are informal estimates.

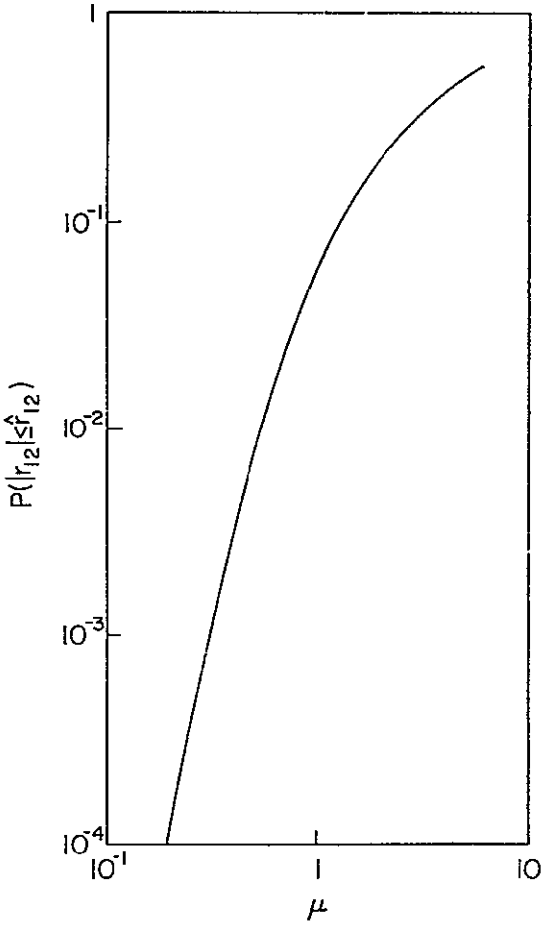

Figure 1.
Tyler, "Comparison..

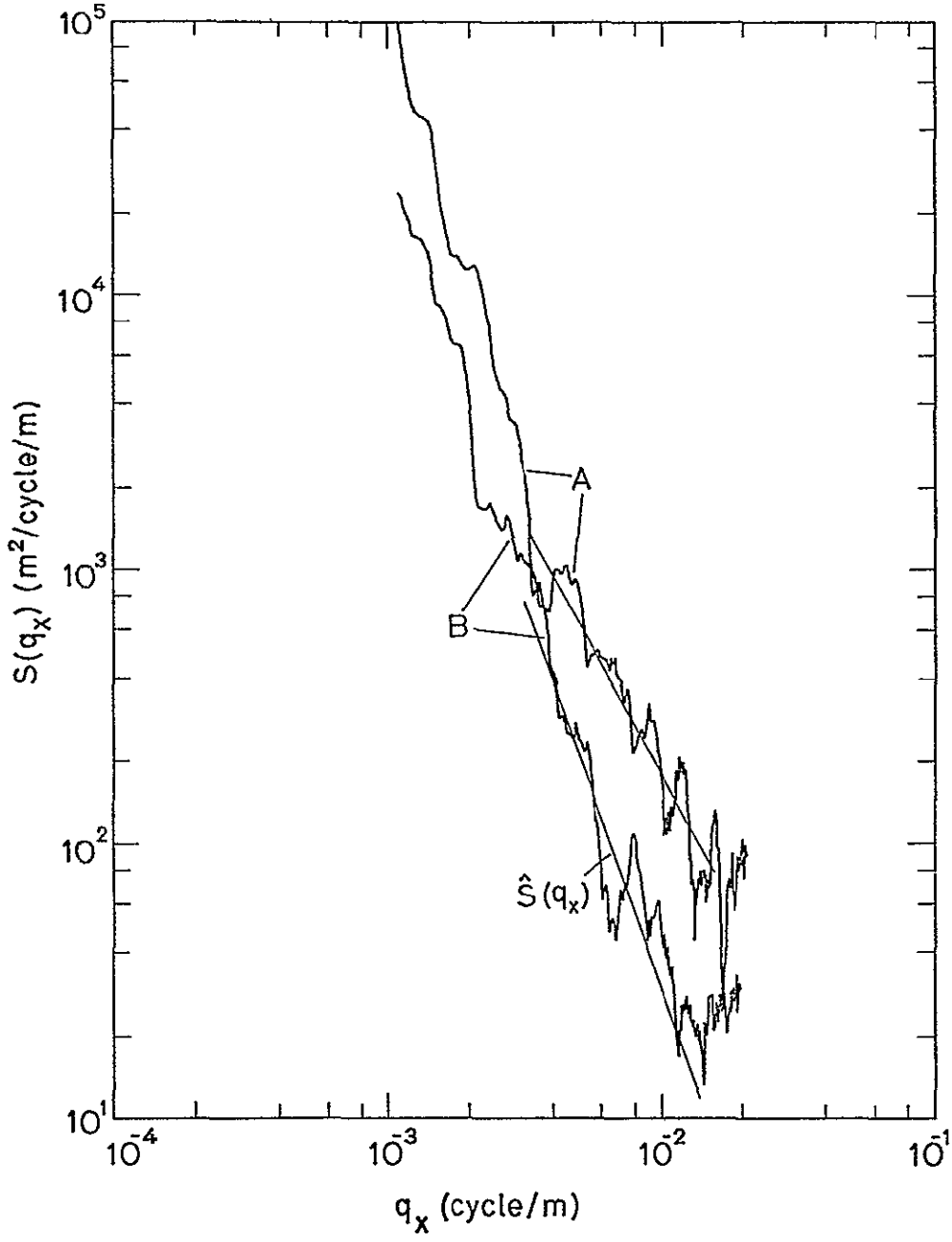

Figure 2.
Tyler,"Comparison..

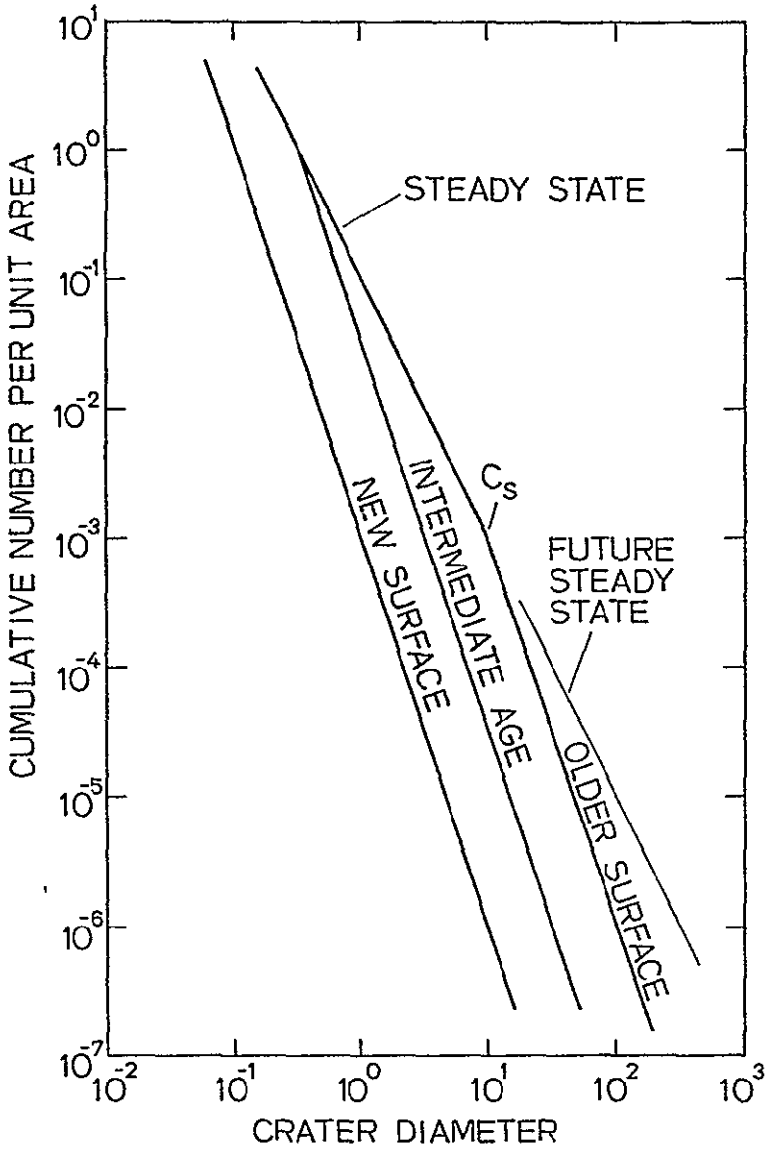

Figure 3.
Tyler, "Comparison..

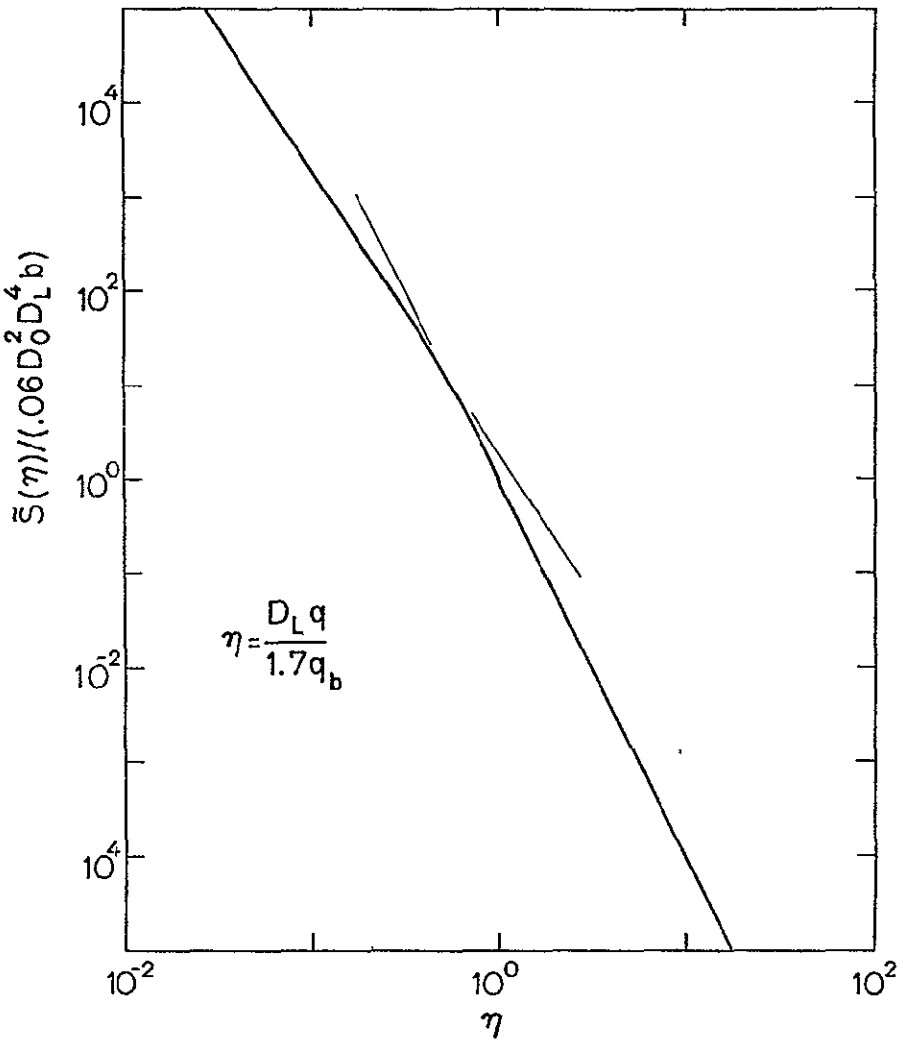

Figure 4.
Tyler, "Comparison..

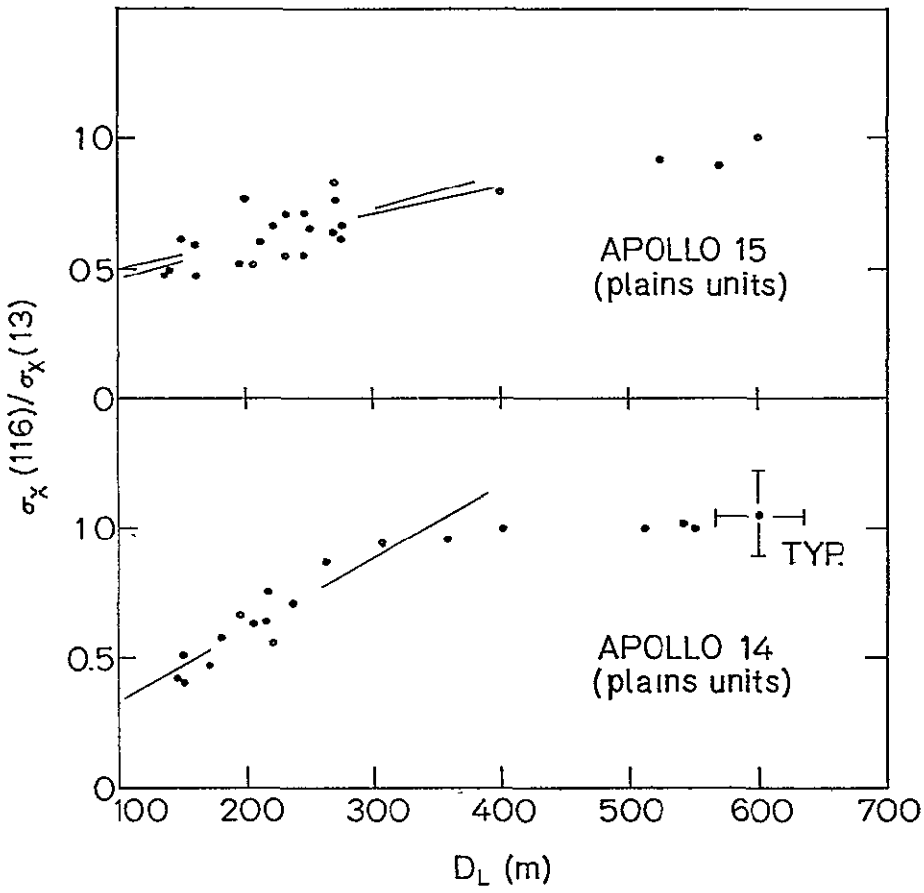

Figure 5.
Tyler,"Comparison...